LAWRENCE
LIVERMORE
NATIONAL
LABORATORY

LLNL-JRNL-589234

Comparison and analysis of zinc and cobalt-based systems as catalytic entities for the hydration of carbon dioxide.

E. Y. Lau, S. E. Wong, S. E. Baker, J. P. Bearinger, L. Koziol, C. A. Valdez, J. H. Satcher, R. D. Aines, F. C. Lightstone

October 8, 2012

PLoS ONE

Disclaimer

Comparison and analysis of zinc and cobalt-based systems as catalytic entities for the hydration of carbon dioxide.

Edmond Y. Lau, Sergio E. Wong, Sarah E. Baker, Jane P. Bearinger, Lucas Koziol,

Carlos A. Valdez, Joseph H. Satcher Jr, Roger D. Aines* and Felice C. Lightstone*

Physical and Life Sciences Directorate, Lawrence Livermore National Laboratory,

7000 East Ave, Livermore, CA 94551.

Abstract

Carbon dioxide (CO_2) sequestration is an application of high interest due to the pressing need to capture large-scale, megaton quantities of this gas from industrial processes or the atmosphere. For this reason, research efforts have been directed towards the development of catalysts that can facilitate this process and thus have a beneficial environmental impact. In nature, the zinc metalloenzyme carbonic anhydrase II (CAII) efficiently catalyzes the conversion of CO_2 to bicarbonate under physiological conditions. Whereas several small molecule mimics of CAII have been synthesized over the years in order to duplicate the enzyme's efficiency, these efforts have met very limited success. Herein, we undertook quantum mechanical calculations of four such mimetics, 1,4,7,10-tetraazacyclododedacane, 1,5,9-triazacyclododedacane, tris(4,5-dimethyl-2-imidazolyl)phosphine, and tris(2-benzimidazolylmethyl)amine, in their complexed form either with the Zn^{2+} or the Co^{2+} ion and studied their reaction coordinate for CO_2 hydration. These calculations demonstrated that the ability of the complex to firmly maintain a tetrahedral geometry and bind bicarbonate in a unidentate manner were necessary requirements for the hydration reaction to proceed favorably. Furthermore, these calculations show that the catalytic activity of the examined zinc complexes was insensitive to coordination states for zinc, while coordination states above four were found to have an unfavorable effect on product release for the cobalt counterparts.

Introduction

In recent years a growing awareness of carbon dioxide atmospheric levels sparked interest in developing rapid methods for the capture and sequestration of the gas from industrial gas streams.[1] Most industrial separation processes for CO_2 involve a liquid in which the dissolved gas ionizes under highly basic conditions leading to its full dissolution and concomitant adsorption into the medium.[2] The rate limiting step in such processes is well known to be the formation of carbonic acid. The slow kinetics nature of this reaction also hinders the uptake of CO_2 in the ocean, and it is the underlying cause of the significant mass transfer limitation at the water's surface.[3] This mass transfer limitation also applies to industrial gas separations[4,5,6] and results in overall decreases by a factor of 1000-fold over that which could be obtained if the hydration of the CO_2 was not the rate-limiting step. Accelerating such processes through the use of catalysts or enzymes would permit smaller and less expensive separation processes to remove CO_2 from industrial gas emissions[7] and could conceivably be fast enough to permit removal of CO_2 from the atmosphere in processes of the type envisioned by Elliot *et al*[8] and Keith *et al.*[9]

In biological systems the reversible hydration of CO_2 to bicarbonate is carried out with formidable efficiency by the zinc metalloenzyme, carbonic anhydrase (CA).[10] In humans, carbonic anhydrase II (CAII, EC 4.2.1.1) is the most efficient isoform exhibiting activity that approaches diffusion limited kinetics. The reaction is catalyzed by a zinc-hydroxide containing center that is formed upon deprotonation of a water molecule coordinated to the active site's zinc ($Zn\text{-}OH_2$, pK_a ~7).[11] The reaction mechanism, which follows ping-pong kinetics, occurs via two independent steps.[10,12] In step one, the zinc-hydroxide in the active site of CA nucleophilically

attacks CO_2 to form a Zn^{2+} bound bicarbonate intermediate whose reaction with water results in the expulsion of bicarbonate.

$$E\text{-}OH^- + CO_2 \leftrightarrows E\text{-}HCO_3^- \xrightarrow{H_2O} E\text{-}H_2O + HCO_3^- \qquad (1)$$

In the second step, the zinc bound water is deprotonated by a nearby histidine (His64 in human CAII) regenerating the catalytic species while the proton is shuttled into the bulk solvent.

$$E\text{-}H_2O + B \leftrightarrows E\text{-}OH^- + BH^+ \qquad (2)$$

Deprotonation of the water is the rate-limiting step in carbonic anhydrase.[12] The extremely high hydration turnover of CO_2 by human CAII is ~10^6 sec^{-1} at pH 9 and 25° C.[11,13] The reverse reaction, dehydration of bicarbonate occurs when the solution pH is below 7.

The X-ray crystal structures of different CAs have been solved and studied in great detail.[10] Crystallographic studies of human CAII show that the enzyme is a monomeric protein consisting of 260 residues. The funnel-shaped appearance of the active site ends with the zinc metal located in its very interior and tetrahedrally coordinated by three histidines (His94, His96, and His119) and a water/hydroxide molecule.[14,15] The active site can be divided into a hydrophobic half (Val121, Val143, Leu198, and Trp209) necessary for CO_2 binding and a hydrophilic half (His64 and Thr199) possessing residues and water molecules intimately involved in an intricate hydrogen bonding network for efficient proton shuttling during the last step of the catalysis. Other divalent metals (Cu^{2+}, Hg^{2+}, Fe^{2+}, Cd^{2+}, Ni^{2+}, Co^{2+} and Mn^{2+})[16] can bind to CAII, but only Co^{2+} has near wild-type catalytic efficiency (k_{cat}/K_m = 8.7 x 10^7 $M^{-1}s^{-1}$ for Zn^{2+} vs 8.8 x 10^7 $M^{-1}s^{-1}$ for Co^{2+}) although the individual k_{cat} and K_m values for CAII differ

when binding the two metal ions.[17] Due to the lack of spectroscopic signatures by the Zn^{2+} ion, its divalent counterpart Co^{2+} has played an important role in studying CA not only because it also utilizes metal-hydroxide catalysis and retains near wild-type activity but it also acts as a spectroscopically active tag.[18]

Despite the merits of CAII, current research into the use of carbonic anhydrase for industrial CO_2 capture has faced significant challenges mainly due to the challenging task of producing a viable enzyme for the rigorous demands encountered in industrial processes. Trachtenberg et al[7,19] have reported the use of a membrane-countercurrent system originally designed for spacecraft use, and Bhattacharya et al[20] developed a spray system containing carbonic anhydrase. Azari and Nemat-Gorgani[21] examined means of using the reversible unfolding of the enzyme, caused by heat, to attach it to more sturdy substrates for industrial use. Lastly, Yan et al[22] incorporated single carbonic anhydrase molecules in a spherical nanogels resulting in improved temperature stability of the enzyme with only moderate loss of activity. Another route of exploration and one that has been undertaken by several groups is to synthesize small molecules capable of mimicking the enzyme's catalytic property. Creating such mimetics requires incorporating key structural features from the enzyme scaffold and avoiding possible degradation mechanisms of the catalytic center. Fortunately, CA mimetics were developed to study the enzyme's reaction mechanism, and several examples of small molecule CA mimetics exist.[23] In the small molecule mimics developed to date, the most prominent features of the enzyme's catalytic site, namely the nitrogen atoms belonging to the histidine side chains, have been used as guiding factors in their design. These nitrogen atoms may be part of an imidazole group,[24] such as tris(4,5-di-n-propyl-2-imidazolyl)phosphine or nitrilotris(2-benimidazolylmethyl-6-sulfonate), or simply secondary amines, as in to case of 1,4,7,10-

tetraazacyclododecane[25] or 1,5,9-triazacyclododecane[26] which chelate the a metal ion to form the catalytic species (Figure 1). These four small molecule mimetics when chelated with Zn^{2+} have been reported to catalyze the hydration of CO_2, although with a more modest catalytic activity compared to the enzyme.

In this *ab initio* study, we have examined carbon dioxide hydration as catalyzed by 1,4,7,10-tetraazacyclododedacane (**N4**), 1,5,9-triazacyclododedacane (**N3**), tris(4,5-dimethyl-2-imidazolyl)phosphine (**Ph**), and tris(2-benzimidazolylmethyl)amine (**Ben**) chelating both Zn^{2+} and Co^{2+} to investigate the reaction mechanism of these two metals and determine the cause for the difference in activity seen in human CAII.

Methods

Quantum mechanical calculations

The hydration reaction of CO_2 catalyzed by **N3**, **N4, Ph,** and **Ben** chelating Zn^{2+} and Co^{2+} was investigated using quantum mechanical calculations. All calculations were carried out using the programs Gaussian03 and Gaussian 09.[27] Geometry optimizations were performed at the B3LYP/6-311+G* level of theory.[28] The catalytically active form of cobalt in carbonic anhydrase is experimentally known to be a high spin quartet (S=3/2).[29] Thus, calculations on the cobalt-containing mimics were carried out with a fixed quartet multiplicity. The stability of the wavefunction was determined by using the STABLE option within Gaussian. The counterpoise method of Boys and Bernardi was used to account for basis set superposition error (BSSE).[30] To test the suitability of the B3LYP functional for these calculations, full optimizations of **N4**-metal

reaction were performed using a recent functional (MPWLYP1M/6-311+G*) that has been successfully used for several organometallics (see supplementary material, Figure S1).[31] Harmonic frequency calculations were performed on all the structures to characterize the stationary points. Transition states were characterized by a single imaginary frequency. The calculated zero-point energies (ZPE) were not scaled. To investigate the effects of solvation on the hydration reaction, single point calculations using the gas-phase geometries were carried out using a conductor-like polarizable continuum model (CPCM)[32] to approximate solvent effects (water, $\varepsilon = 78.4$). It has been shown that the solvation free energies from single point PCM calculations using gas-phase geometries from density functional calculations are in reasonable agreement with values obtained from full optimizations.[33] All solvation calculations used the simple united atom topological model (UA0)[34] using UFF radii.[35] The gas phase zero point energies were included in the solvation calculations. Natural population analysis was performed on the optimized structures to assess the charge distributions on these complexes.[36]

Synthesis

Tris(6-sulfobenzimidazolylmethyl)amine (Ben). The ligand was synthesized following a previously published protocol for the synthesis of tris-benzimidazole-based compounds.[37] Thus, 4-sulfo-1,2-diaminobenzene[38] (4.0 g, 21.2 mmol) was transferred into a 250 mL round bottom flask equipped with a large stir bar. The solid was made into suspension with the addition of ethylene glycol (120 mL). To the suspension, nitrilotriacetic acid (1.13 g, 5.89 mmol) was added in one portion, the flask equipped with a condenser (set with water at 10^{o} C) and the resulting mixture heated to 210^{o} C using a sand bath overnight. After 18 hours of

heating, the flask was removed from the sand bath and the black-colored reaction mixture allowed to cool down to ambient temperature. The mixture was subsequently poured into a 1000 mL Erlenmeyer flask containing ice water (300 mL) in small portions with constant swirling. The grey precipitate was collected using vacuum filtration and washed copiously with cold, deionized water (5 x 50 mL), and dried under vacuum to afford the title compound (2.90 g, 74%). The sodium salt of the ligand was obtained by reacting the ligand (1.0 g, 1.5 mmol) with NaOH (180 mg, 4.5 mmol, 3.05 equiv. to ligand) in deionized water (10 mL). The water was evaporated under reduced pressure to yield a light grey solid (1.03 g, 97%). ^{1}H NMR (600 MHz, D_2O) δ 7.94 (s, 3H), 7.53 (d, J = 8.5, 3H), 7.35 (d, J = 8.5, 3H), 4.07 (s, 6H); ^{13}C NMR (150 MHz, D_2O) □ 155.4, 139.6, 137.9, 136.5, 119.7, 114.6, 112.8, 53.2; Anal. ($C_{24}H_{18}N_7Na_3O_9S_3$•$H_2O$) C, 39.40; H, 2.76; N, 13.40; Found: C, 39.32; H, 3.08; N, 13.49. The characterization of the zinc complex and the protocols for the kinetic analysis for Ben can be found in the supplementary materials.

Results and discussion

Our *ab initio* calculations investigated the hydration of CO_2 catalyzed by the Zn^{2+} containing catalysts (Figure 1). The hydration of CO_2 by carbonic anhydrase and mimetics is believed to follow the same reaction pathway. Thus, the catalytic cycle begins with nucleophilic attack on the CO_2 by the zinc-hydroxide species to form Zn^{2+}-bicarbonate intermediate followed by displacement of the bicarbonate from Zn^{2+} by water; the water then loses a proton to regenerate the catalysis. Cobalt substituted carbonic anhydrase also utilizes the above metal-hydroxide reaction mechanism for CO_2 hydration, but it has ~50% of the catalytic activity

exhibited by the wild-type enzyme.[17] To gain insight in the possible fine differences between the two metals, chelators containing Co^{2+} were also studied. The cobalt complexes are assumed to be in alkaline conditions which favor tetrahedral geometries and share similar characteristics to the zinc complexes.[39] There have been several *ab initio* studies on the hydration of CO_2 by CAII[40] but a thorough comparative study between Zn^{2+} and other metals ions within CAII have not been as widely studied.[41] Additionally, tris(4,5-di-n-propyl-2-imidazolyl)phosphine catalyzes the hydration of CO_2 but the non-catalytic tris(4,5-dimethyl-2-imidazolyl)phosphine (**Ph**) it was chosen for computational tractability and can provide insights into the reaction mechanism.

Nucleophilic Attack of CO_2

The first step of the catalyzed hydrolysis of CO_2 in the gas-phase is formation of an encounter complex (EC) between the separated reactants (Figure 2). The EC is formed when CO_2 interacts weakly with one of the amine hydrogens in the ring structure of the macrocycles **N3** and **N4**. Due to the lack of N-H moieties around the catalytic OH^- group in the **Ph** and **Ben** ligands only form van der Waals complexes with CO_2. The stabilization energy is approximately -1 to -4 kcal/mole for each of the Zn^{2+} and Co^{2+}encounter complexes relative to the separated reactants (see Figures 3A and 3B). The **N3** and **N4** ECs were found to have greater stabilization energies than the **Ph** and **Ben** ECs. The amine hydrogen to CO_2 oxygen distances were measured to be 2.071 and 2.124 Å for **N3**-Zn and **N4**-Zn, respectively, while the Co^{2+} complexes had similar distances of 2.090 (**N3**-Co) and 2.322 (**N4**-Co). Additionally, the angle formed by the CO_2 oxygen with the hydrogen and nitrogen of the amine (O••• H-N) of **N3** and

N4 shows that the CO_2 is likely not forming a strong hydrogen bond. Both **N3** M^{2+}-complexes have angles close to 180° whereas the **N4** complexes possess angles of 137° for Co^{2+} and 158° for Zn^{2+}. The distances between the CO_2 carbon and the M^{2+}-hydroxide oxygen were 2.674 (**N3**) and 2.640 Å (**N4**) for the Zn^{2+} EC structures respectively, while the Co^{2+} complexes had slightly longer distances. The value obtained for **N3**-Zn is similar to that obtained by Brauer et al. obtained at the HF/6-311+G* level of theory while our **N4**-Zn value is almost 0.1 Å shorter than Brauer's value.[42] Calculations using the B3LYP or MPWLYP1M functional provide similar results for both M^{2+}-complexes. Only minor differences in the energies and geometries were found for the **N4** reaction with either Zn^{2+} or Co^{2+} between these fully optimized calculations (Supplementary Material, Figure S1).

The calculated distances for the EC structures are in reasonable agreement with a recently solved crystal structure of human carbonic anhydrase (HCAII) with CO_2.[43] In this crystal structure (PDB ID 3D92), the CO_2 carbon to Zn^{2+}-hydroxide oxygen distance is 2.791 Å. The CO_2 is bound in a hydrophobic pocket within HCAII and one of its oxygens interacts with the amide backbone nitrogen of Thr199 (3.493 Å). Interestingly, the same study also showed that a metal ion is not even necessary for CO_2 to bind in the correct location in the HCAII active site. Although **Ph**-metal and **Ben**-metal complexes lack an N-H group to stabilize the CO_2 around the ligands, the distance from the M^{2+}-hydroxide oxygen to the CO_2 carbon was comparable to the **N3** and **N4** ligands even though their stabilization energy is smaller (see Figure 2). Natural population analysis (NPA) of the complexes show that there is little charge difference between Zn^{2+} in **N3** or **N4** (supplementary material, Table S1), a finding that is consistent with the work of Brauer *et al*.[42] Two additional pieces of information obtained from NPA are: (1) there exists

some charge polarization occurring in the CO_2 molecule from its interaction with the amine and (2) the Zn^{2+}-hydroxide is more nucleophilic in nature than its Co^{2+} counterpart.

The first transition state (TS1) in the hydration reaction is formed when the distance between the M^{2+}-hydroxide oxygen to the carbon of CO_2 falls below 2 Å. In the Co^{2+} complexes, the distances for the **N3**-Co, **N4**-Co, **Ph**-Co, and **Ben**-Co transition states were 1.767, 1.870, 1.777, and 1.720 Å, respectively (see Figure 2). The **N3**-Zn complex has a similar transition state distance to **N3**-Co of 1.732 Å, but the **N4**-Zn structure has a much shorter distance of 1.660 Å relative to **N4**-Co. The reaction barriers are similar for **N3**-Zn, **N4**-Zn, and **N3**-Co (~12 kcal/mole) while the reaction barrier for **N4**-Co is significantly lower at 7.2 kcal/mole (Figure 3). The difference in energy is due to an earlier transition state for **N4**-Co than found in the other complexes. Although the CO_2 to M^{2+}-hydroxide distance in **N4**-Co is longer than in **N4**-Zn, the oxygen in CO_2 shows greater coordination to Co^{2+} (2.353 Å) relative to Zn^{2+} (2.428 Å). The TS1 geometry for both **Ph**-metal structures are similar. The distance between the hydroxyl oxygen and carbon of CO_2 is 1.744 for **Ph**-Zn. Both **Ben**-metal structures had late transition states that lead to high activation barriers for the final formation of bicarbonate (~13 kcal/mole). There is minimal change in the charge on either metal in going from EC to TS1 except for **Phen**-Co. When TS1 is formed, the charge on the hydroxyl oxygen drops to almost the same values (ranging from -1.02 to -1.09 |eu|) for all eight complexes even though the Zn^{2+} complexes was found to possess higher charges in the EC structures (supplementary material, Table S1).

After passing the first transition state, a bicarbonate complex directly chelated to the metal is formed. There has been great deal of debate about the actual conformation of the

bicarbonate around the metal center in carbonic anhydrase. From these calculations and others, that a Lindskog intermediate (OH of bicarbonate is oriented towards the metal) will clearly be formed first in this reaction (denoted I1).[41b,42,44] The geometry of both **N3** complexes is very similar with one oxygen directly coordinated to the metal center (1.886 Å and 1.900 Å, for Co^{2+} and Zn^{2+}, respectively) and the bicarbonate hydroxyl group weakly interacting with the metal ion (2.972 Å and 2.949 Å, for Co^{2+} and Zn^{2+}, respectively). The geometry around the metal is tetrahedral. Similar asymmetrical bicarbonate coordination geometries for I1 were obtained for the **Ph** and **Ben** complexes for both metal ions (see Figure 2). The **N4**-Zn structure resembles the **N3**-metal structures with a single oxygen coordinated to Zn^{2+}, and the hydroxyl group asymmetrically interacting with the zinc (1.909 and 2.933 Å). The I1 **N4**-Co geometry differs from the other complexes. The oxygens coordinating Co^{2+} are much more symmetrical. The metal to coordinating oxygen distance is 1.976 Å, and the hydroxyl oxygen is 2.398 Å away. Although not perfectly octahedral, this structure shows cobalt's ability/preference to coordinate six ligands.

Rotation about the oxygen bond coordinated to the metal center in the Lindskog intermediate (I1) leads through a shallow transition state (TS2) to the lower energy Lipscomb intermediate (I2), which has both carboxylate oxygens of bicarbonate directed towards the metal. This second transition state occurs when the dihedral angle (OC – C, see Figure 1C) has rotated approximately 90°. For both metal ion complexes of **N3, Ph,** and **Ben** structures, TS2 has almost identical geometries. Interestingly, the TS2 structures for **N4** differ significantly (Figure 4). **N4**-Zn has a transition state that resembles the **N3** structures, but the **N4**-Co TS2 structure still shows a preference for octahedral binding even though one site is unoccupied. It should be pointed out that proton transfer from the hydroxyl oxygen (OH) of bicarbonate to the non-coordinated

oxygen (O) is also a viable mechanism for conversion of I1 to I2 but requires additional water molecules for this to have an activation barrier as low as bond rotation.[45] In either case, this portion of the reaction is not expected to be rate-limiting.

The initial Lipscomb intermediates for both **N3** complexes are similar; a single oxygen is coordinated to the metal, and the other carboxylate oxygen is weakly coordinated to the metal (1.920 and 2.964 Å for Zn^{2+} and 1.905 and 3.027 Å for Co^{2+}). Bidentate binding geometries for bicarbonate to the metal were also obtained and are ~0.9 kcal/mole higher in energy than the I2 structure. The I2 geometry is disrupted by formation of a hydrogen bond between one carboxylate oxygen and an amine within the macrocycle. The carboxylate oxygens to metal distances are (1.924 Å, 2.982 Å) and (1.909 Å, 3.039 Å) for Zn^{2+} and Co^{2+}, respectively for unidentate geometries. For the **N4** complexes, the carboxylates of bicarbonate are also bound differently in the Lipscomb intermediate depending on the metal. For **N4**-Zn, the oxygen to zinc distances are 1.930 and 2.909 Å which is similar to the values for the unidentate **N3**-Zn complex. For **N4**-Co, the oxygen cobalt distances are almost identical at 2.113 and 2.158 Å, again reflecting cobalt's preference for an octahedral geometry in this macrocycle. The bicarbonate geometries for the **Ph** compounds were unidentate for Zn^{2+} but bidentate for Co^{2+}. These calculated results are in good agreement with crystal structure data of Zn^{2+} and Co^{2+} bound by a tris(pyrazoyl)hydroborato ligand and coordinating nitrate or carbonate.[46] In the Zn^{2+} compounds, only one nitrate or carbonate oxygen binds to the metal at a distance of 1.98 Å, and the second oxygen is greater than 2.6 Å from the metal. For the Co^{2+} compounds, the two oxygens bind more symmetrically around the metal at 2.001 and 2.339 Å for nitrate and 2.055 and 2.271 Å for carbonate in the crystal structures. The bicarbonate I2 geometries for the **Ben**

compounds were almost identical. Both metals bind the bicarbonate in a unidentate geometry with oxygen distances of 1.936 and 3.187 Å for Zn^{2+} and 1.934 and 3.198 Å for Co^{2+}.

The calculated results for nucleophilic attack of CO_2 are in qualitative agreement with model studies. The x-ray crystal geometries of tris(pyrazolyl)hydroborato zinc hydroxide and cobalt hydroxide complexes are similar to those obtained for the **N3** complexes.[47] These structures all have tetrahedral geometries around the metal center and readily react with CO_2 to form bicarbonate. Unfortunately, the tris(pyrazolyl)hydroborato complexes are not soluble in water therefore release of the metal bound bicarbonate is not possible with these catalysts.

Product Release

To study the release of bicarbonate from the metal center, a single water molecule was added to the I1 (Lindskog) and I2 (Lipscomb) structures since it was not obvious which geometry would have the lower activation barrier for product release. Once a water molecule was added to each intermediate, the structures were reoptimized. In all cases, the I2 structure with water was the lower energy structure. The water molecule was stabilized by formation of a hydrogen bond between the oxygen of water (OW) and the hydrogen from the amine group in the ring structure of both **N3** and **N4** and interaction of a hydrogen from water (H1) with the oxygen of bicarbonate (OC) coordinating the metal (see Figure 5). For the **Ph** and **Ben** structures, the water hydrogen bonds with the bicarbonate but likely does not interact strongly with the rest of the complex since there are no other polar group in the vicinity. Interestingly, the structure obtained for the **Ph**-Zn is very similar to the x-ray structures of 2VVB[48] and

1XEG,[49] where a unidentate bicarbonate or acetate is interacting with one water molecule. The original intermediate structures were not significantly affected by the inclusion of the water molecule**.** In the case of **N3**-Zn, the I2 structure becomes unidentate and resembles I2 for the other complexes. For **N3**-Co, the second oxygen distance elongates to 2.465 Å to Co^{2+}. The energy difference of I1 relative to I2 did not change significantly by adding the water molecule.

Unlike the macrocycles, lower energy structures than the encounter complex were found when the water molecule directly coordinates to the metal ion for both **Ph** and **Ben** complexes. When the water coordinates to metal in the **Ph** complex, a trigonal bipyramidal metal center is formed. Two conformers are possible in the case of zinc, the lowest energy structure has the water in the axial position and the bicarbonate (in the equatorial position) hydrogen bonds to the coordinated water (Figure 6). Although it is possible to obtain a minimum energy structure with bicarbonate in the axial position and water equatorial, the energy barrier separating these two structures disappears when the ZPE correction is included. A turnstile pseudorotation occurs to transform one structure to the other, but the amount of rearrangement to have the bicarbonate go from axial to equatorial is small because of the three-fold symmetry of the phosphine complex (supplementary material, Figure S3). Both ligands only need to rotate by ~60° to interconvert between conformations. Similar coordination of water and bicarbonate around the zinc has also been observed in carbonic anhydrase II binding acetate.

In the wild-type (WT) protein (PDB, 1CAY), the coordination around the zinc was a distorted trigonal bipyrimid with a water as an equatorial ligand and the acetate as an axial ligand (Figure 7).[50] Comparison of the WT enzyme with the T199A mutant (PDB, 1CAM) shows that the hydroxyl group of T199 is important in the positioning of the water molecule coordinated to the zinc (supplementary material, Figure S3).[51] The positioning of the water and the bicarbonate

around the zinc by Thr199 likely creates a situation in which the geometry is not optimal and makes release of bicarbonate more favorable. The Zn-carboxylate oxygen distances for the WT and T199A proteins are 2.42 and 2.27 Å, respectively. In the 1CAM crystal structure, the angle formed by the His94 NE2 – Zn – O of water is 136.6°. The analogous angle in 1CAY is 110.0°. Experimentally, the T199A mutant is ~100 times slower at turning over CO_2 than the WT enzyme, and the binding of inhibitors such as thiocyanate and bicarbonate is enhanced by 20-fold.[52] In the E106Q mutant protein (PDB, 1CAZ),[50] the zinc coordination is trigonal bipyramidal, but the water and acetate coordination is now reversed with water as the axial ligand and acetate as the equatorial ligand. Bicarbonate is more strongly coordinated to the Zn^{2+} in the equatorial position (Zn-O bond is 1.953 Å) relative to the axial position (Zn-O bond is 2.050 Å) in **Ph**-Zn. Calculations of **Ph**-Zn showed this to be the low energy conformation of the trigonal bipyramidial geometry. The carboxylate sidechain of E106 is important for positioning the water around the zinc to avoid this conformation since the E106D mutant shows little change in activity from the wild-type enzyme. The amide sidechain of E106Q rotates away from T199 and functions as a hydrogen donor with T199 instead of an acceptor. This changes the hydrogen bonding network within the active site, resulting in a 1000-fold decrease in the maximal rate for the E106Q mutant.[52]

The **Ph**-Co encounter complex is a distorted trigonal bipyramidal structure with water in the axial position and bicarbonate in the equatorial position. One oxygen of the bicarbonate is hydrogen bonding with the water molecule. This complex could also be described as having an octahedral geometry but missing the sixth ligand. Interestingly, a formal octahedral complex 3.6 kcal/mole higher in energy relative to the pentacoordinate structure was also obtained. This structure which has two oxygens of the bicarbonate equatorially coordinated to Co^{2+} and water at

the axial position is almost identical to the Co^{2+} carbonic anhydrase binding bicarbonate (PDB 1CAH)[53] (Figure 8) and also the structure of cobalt tris[2-isopropylimidazol-4(5)-yl]phosphane coordinating to nitrate and water.[54] A similar octahedral structure was also obtained for the Zn^{2+} complex that was 5.44 kcal/mole higher in energy relative to the I3 structure. The trigonal bipyramidal coordination of the bicarbonate in the enzyme may not be favorable. An overlay of the I3 structure in the active site of 1CAH shows the bicarbonate would be in close contact with the side chain of L198.

Axial and equatorial arrangements for bicarbonate in both **Ben**-metal complexes were also found, but interconversion between these structures was not possible (Figure 9). When water coordinates to the metal, an octahedral complex forms for both **Ben-**metal complexes as the benzimidazole shift positions to take up an equatorial arrangement around the metal. The interconversion of conformation by the turnstile pseudorotation in this case would likely have a high barrier since this complex is not symmetric and would require the water and bicarbonate to exchange positions (180° rotation). The octahedral geometry adopted by the **Ben**-Zn complex is reminiscent of tris(6-amino-2-pyridylmethyl)amine binding Zn^{2+} which catalyzes phosphodiester cleavage.[55] Indeed, complexes of Zn^{2+}, Co^{2+}, and Cu^{2+} coordinated to tris(2-benimidazylmethyl)amine have been shown to catalyze the hydrolysis of p-nitrophenyl acetate.[56]

For product release, an addition-substitution reaction occurs with a water molecule displacing the bicarbonate. At the transition state (TS3), the water molecule coordinates to the metal ion, causing the oxygen of the bicarbonate to weaken (Figure 9 and 10). In the zinc complexes, the oxygen of water is 1.900 Å (**N3**), 2.024 Å (**N4**), 1.961 Å (**Ph**), and 2.049 Å (**Ben**) from Zn^{2+} with the oxygen of the previously coordinated bicarbonate now at 2.938 Å (**N3**), 2.886

Å (**N4**), 2.676 Å (**Ph**), and 2.823 Å (**Ben**). The displaced oxygen of bicarbonate interacts with one of the hydrogens of the water and ultimately abstracts the proton from the water to form carbonic acid and to reform the metal-hydroxide catalyst. The transition state geometry for **N3**-Co is almost identical to **N3**-Zn with the water bound slightly tighter (1.961 Å), and the bicarbonate more weakly bound to the metal (3.017 Å). The transition state for **N4**-Co differs from the other three structures. The water is bound tightly to the Co^{2+} and the oxygen of bicarbonate is still coordinated to the metal (2.509 Å). Additionally, the previously mentioned TS3 structures (both **N3** and **N4**-Zn) had the oxygen of bicarbonate interacting with one of the hydrogens on the water molecule. In the TS3 structure of **N4**-Co, the hydrogen/proton from the water has transferred to the bicarbonate to form carbonic acid. No change in the ring structure occurred for either **N4** complex at the transition state.

From these calculations, **Ben**-Zn should be a poorer catalyst at CO_2 hydration that **N3** or **N4,** although the water soluble sulfonated version of **Ben**-Zn was reported to be a highly active at low temperatures, and its activity was extrapolated to room temperature.[57] Interestingly, no direct kinetic measurements for the sulfonated **Ben**-Zn were reported at room temperature. To better understand the catalytic properties of **Ben**-Zn, the sulfonated benzimidazole compound was synthesized and tested. The sulfonated benzimidazole did not show any catalytically properties at room temperature and had slight activity at 50° C (supplementary materials) which was consistent with the calculated activation barrier for **Ben**-Zn.

For all complexes, the transition state from the I2 structure was lower in energy than the transition state from the I1 structure. Interestingly, the activation barrier from I1 or I2 to their respective transition states was almost identical in value. The activation barrier for bicarbonate

release range from a low value of 14.8 kcal/mole for **N4**-Zn to a high of 20.7 kcal/mole for **Ben**-Co. From these calculations, product release is the rate-limiting step for the hydration of CO_2. These values differ from those obtained by Mauksch et al. using the model system $[(NH_3)_3Zn(OH)]^+/CO_2$.[58] They find that nucleophilic attack is the rate-limiting step for CO_2 hydration and only a small barrier for product release. This discrepancy is due to their assumption that one of the protons on the coordinated water molecule transfers to the bicarbonate while both are still coordinated to the zinc. This proton transfer seems unlikely in solution from pKa measurement of the macrocycle triamine [2-(2-hydroxyphenyl)-1,5,9-triazacyclododecane coordinated with zinc.[59] This macrocycle is pentacoordinated with a trigonal bipyramidal geometry. The 2-hydroxyphenyl moiety has a pKa of 6.8, and the coordinated water has a pKa of 10.7. Having a charged oxygen coordinated to the zinc reduces the metal's ability to acidify the water molecule since the pKa of water bound to 1,5,9-triazacyclododecane-zinc is 7.5. The calculated activation barriers for the zinc complexes for **N4** (14.8 kcal/mole), **N3** (15.7 kcal/mole), **Phen** (15.6 kcal/mole), and **Ben** (18.3 kcal/mole) are in reasonable agreement with measured rate constants for CO_2 hydration 2494 M^{-1} S^{-1},[60] 1083 M^{-1} S^{-1},[60] 898 M^{-1} S^{-1},[61] and not catalytic, respectively, The correlation between product release and experimental rate constants is consistent with our previous results, showing the bond dissociation energy between bicarbonate and Zn-azamacrocycles corresponds with the experimental results.[60]

The calculated hydration reaction catalyzed by the tetrahedral coordinating **N3,** using either Zn^{2+} or Co^{2+}, was very similar in both geometries and energies obtained. This is consistent with experimental results that show almost identical coordination geometries and wild-type activity for alpha-class carbonic anhydrases that have Zn^{2+} substituted with Co^{2+}.[62,17] The calculated activation barrier for release of bicarbonate is high in these polyamine complexes yet

HCAII experiments have shown this step in the reaction to be rapid and not rate-limiting.[63] In HCAII, both experiment and theory have shown that Thr199 has a destabilizing effect on bicarbonate binding to zinc.[52,64,65]65 Hybrid QM/MM calculations by Merz and Banci show that the active site of HCAII promotes destabilization by pulling one of the carboxylate oxygens of bicarbonate away from the zinc by formation of a hydrogen bond with the hydroxyl group of Thr199.[65] Using PM3 calculations, they found that having the zinc-bicarbonate active site geometry destabilizes the Lipscomb intermediate by 8.7 kcal/mole relative to the QM optimized structure. These results are also qualitatively in agreement with estimated free energies from kinetics data for carbonic anhydrase that show dissociation of bicarbonate limits the CO_2 hydration catalyzed by HCAI and the Thr200His mutant of HCAII.[66]

Solvent effects on CO_2 hydration

To estimate the effects of solvent on the CO_2 hydration reaction, single-point conductor-like polarization continuum model (CPCM) calculations were performed on the optimized gas-phase geometries. Addition of solvation effects removes the encounter complex as a minimum along the reaction coordinate (see Figure 11). The separated reactants go directly to the first transition state and the activation barrier is significantly lowered. The activation barrier ranged from 0.21 to 3.16 kcal/mole. Once past the transition state the bicarbonate is formed. When including solvation effects the energy differences between the Lindskog (I1) and Lipscomb (I2) intermediates are much smaller. In the gas-phase the energy difference was ~5 kcal/mole or greater but in solution the energy differences are reduced and ranged from 0.18 to 2.31 kcal/mole. Addition of a water molecule to the intermediate structures does not significantly

change the energy difference between the two geometries for the CPCM calculations. In some cases, the activation barrier for interconversion of I1 to I2 is the highest barrier. This is likely due to this transition state is not involved in two species either forming or separating.

The activation barrier for bicarbonate release is significantly reduced by solvent effects. In the case of the **N3** complexes, the activation barrier is reduced by 12.48 and 11.56 kcal/mole for **N3**-Zn and **N3**-Co, respectively. Solvation in the high dielectric medium makes separation of the two charged species more favorable, and the reduction in the barrier is large enough that in the case of **N3**-metal ion, interconversion of I1 to I2 is rate-limiting. With the inclusion of solvation, the activation barrier for bicarbonate release is almost identical for either the Lindskog or Lipscomb intermediates for both **N3** complexes and **N4**-Zn. The active site of HCAII has a well ordered solvent network that provides a route for proton release to bulk solvent,[67] but this network may also contribute in lowering the barrier for product release. The CPCM activation barriers for product release from Zn^{2+} overestimate the stabilization for the calculated barrier for bicarbonate dissociation in the macrocycles. Loferer et al. using QM/MM methods[68] calculated a barrier of 6.2 kcal/mole for bicarbonate dissociation, and from these calculations barriers of 3.19 (**N3**-Zn) and 4.68 kcal/mole (**N4**-Zn) were obtained. Interestingly, the activation barriers for product release are much higher for **Phen**-Zn (9.40 kcal/mole) and **Ben**-Zn (11.82 kcal/mole).

For **N4**-Co, solvation effects did not significantly reduce the activation barrier for bicarbonate release. It would appear that **N4**-Co does not catalyze the hydration of CO_2 even though it had the lowest barrier for nucleophilic attack. The preference of an octahedral geometry for **N4**-Co makes release of bicarbonate improbable. This is consistent with

experiments that showed a 5-coordinated Co^{2+} complex (four nitrogens and one oxygen from water) is able to form cobalt-hydroxide but does not catalyze the hydration of CO_2.[69] We should also point out that having an additional water molecule coordinated to the cobalt could contribute to lowering the activation barrier or change the coordination of bicarbonate to unidentate, but we did not pursue these calculations since it was beyond the scope of the present study. Clearly, solvation has a significant effect on the activation barrier for product release although the reduction in the barrier could be overestimated, since we are not using optimized CPCM structures.

Conclusions

Models that mimic the reactivity of carbonic anhydrase are of interest not only academically but to industry which is trying to lower the amount of CO_2 being released into the atmosphere.[70] Two of the most successful mimics of carbonic anhydrase are the cyclic polyamines 1,4,7,10-tetraazacyclododedacane (**N4**) and 1,5,9-triazacyclododedacane (**N3),** when coordinated to zinc are able to catalyze the reversible hydration of CO_2. From our calculations, the Zn^{2+} and Co^{2+} complexes of **N3** have very similar coordination geometries to human carbonic anhydrase II and comparable energetics. The **N4**-Zn complex has slightly higher turnover than the **N3**-Zn but has been criticized as a mimic for human carbonic anhydrase II because it has pentacoordinate geometry. Although the coordination differs, the calculations show that **N4**-Zn follows the same reaction as the **N3**-Zn/Co complexes. The **N4**-Co complex is able to lower the barrier for nucleophilic attack more than any of the other complexes by having an octahedral geometry around Co^{2+} but this at the expense of being able to release bicarbonate

later in the reaction. Interestingly, the gamma-class carbonic anhydrase from *Methanosarcina thermophila* (Cam) which normally uses Fe^{2+} to catalyze the hydration of CO_2 may have found a way around this product release problem.[71] This carbonic anhydrase can also utilize pentacoordinated Zn^{2+} or hexacoordinated Co^{2+}, and Co-Cam is actually better at catalyzing the hydration reaction than Zn-Cam.[72] The crystal structure of bicarbonate bound in Zn-Cam and Co-Cam show they have different coordination positions around the metal ion (Figure 12).[73] For Zn-Cam, the geometry of bicarbonate resembles the Lipscomb intermediate for **N3** with the carboxylate oxygens 2.48 and 3.11 Å from Zn^{2+}. In Co-Cam, only one oxygen in bicarbonate is bound to Co^{2+}, and two waters take up the other coordination sites. Interestingly, the geometry of bicarbonate around Co^{2+} most resembles the TS2 structure of **N4**-Co. It would be interesting if a catalyst based on the binding geometry in Cam could be created. If possible, its application to industry could be significant since the susceptibility of Zn-Cam and Co-Cam to anionic inhibitors differs.[74] The difference in the inhibitors is likely due to the coordination preference of the metals.

The activation barriers for **N3**-Zn and **N4**-Zn from our calculations are quite low yet these complexes are ~1000 slower at catalyzing the hydration of CO_2 relative to HCAII. One aspect of the reaction that could not be readily studied is the importance of reactant positioning. Although the rate-limiting step in HCAII is proton loss from the metal bound water, it would not be expect to be limiting for these mimics that are solvent exposed and function optimally at alkaline pH. Recent crystal structures show that HCAII contains a hydrophobic pocket that binds CO_2 in a conformation that will readily react with the zinc-hydroxide.[43] In fact, the presence of a metal is not even required for CO_2 binding in HCAII.[43] Reactant positioning likely is an important aspect of the hydration reaction by HCAII and for these mimics.

Acknowledgements

We thank the Laboratory Directed Research and Development Program at Lawrence Livermore National Laboratory for funding 10-ERD-035. This work performed under the auspices of the U.S. Department of Energy by Lawrence Livermore National Laboratory under Contract DE-AC52-07NA27344. A generous allocation of computer time on Livermore Computing is gratefully acknowledged.

References

[1] R. Pachauri and A. Reisinger, "Climate Change 2007: Synthesis Report," Intergovernmental Panel on Climate Change, 2007.

[2] J. Figueroa, T. Fout, S. Plasynski, H. McIvried, and R. Srivastava, *International Journal of Greenhouse Gas Control*, 2008, **2**, 9-20.

[3] W. Stumm, and J. Morgan, Aquatic Chemistry; 3rd ed.; Wiley-Interscience, 1996.

[4] J. Stolaroff, *Environmental Science and Technology*, 2008, **4**, 2728-2735.

[5] J. Stolaroff, Carnegie Mellon University, 2006.

[6] J. T. Cullinane and G. T. Rochelle, *Ind. Eng. Chem. Res*., 2006, **45**, 2531-2545.

[7] L. H. Bao, and M. C. Trachtenberg, *J. Membrane Sci*., 2006, **280**, 330-334.

[8] S. Elliott, K. S. Lackner, H. J. Ziock, M. K. Dubey, H. P. Hanson, S. Barr, N. A. Ciszkowski, and D. R. Blake, *Geophys. Res. Lett*., 2001, **28**, 1235-1238.

[9] D. Keith, M. Ha-Duong, and J. Stolaroff, *Climatic Change*, 2005, **74**, 17-45.

[10] S. Lindskog, *Pharmacol. Ther*., 1997, **74**, 1-20.

[11] H. Steiner, B.-H. Jonsson, and S. Lindskog, *Eur. J. Biochem*., 1975, **59**, 253-259.

[12] D. N. Silverman and S. Lindskog, *Acc. Chem. Res*., 1988, **21**, 30-36.

[13] R. G. Khalifah, *J. Biol. Chem*., 1971, **246**, 2561-2573.

[14] A. Liljas, K. K. Kannan, P. C. Bergsten, I. Waara, K. Fridborg, B. Strandberg, U. Carlborn, L. Jarup, S. Lovgren, and M. Petef, *Nat. New Biol.*, 1972, **235**, 131-137.

[15] K. Hakansson, M. Carlsson, L. A. Svensson, and A. Liljas, *J. Mol. Biol*., 1992, **227**, 1192-1204.

[16] S. Lindskog and P. Nyman, *Biochim. Bipohys. Acta*, 1964, **85**, 462-474.

[17] K. A. Kogut and R. S. Rowlett, *J. Biol. Chem*., 1987, **262**, 16417-16424.

[18] I. Bertini and C. Luchinat, *Acc. Chem. Res*., 1983, **16**, 272-279.

[19] R. M. Cowan, J. J. Ge, Y. J. Qin, M. L. McGregor and M. C. Trachtenberg, *Ann. NY. Acad. Sci*., 2003, **984**, 453-469.

[20] S. Bhattacharya, A. Nayak, M. Schiavone and S. K. Bhattacharya, *Biotechnol. Bioeng.*, 2004, **86**, 37-46.

[21] F. Azari and M. Nemat-Gorgani, *Biotechnol. Bioeng.*, 1999, **62**, 192-199.

[22] M. Yan, Z. X. Liu, D. N. Lu and Z. Liu, *Biomacromolecules*, 2007, **8**, 560-565.

[23] V. M. Krishnamurthy, G. K. Kaufman, A. R. Urbach, I. Gitlin, K. L. Gudiksen, D. B. Weibel and G. M. Whitesides, *Chem Rev*., 2008, **108**, 946-1051.

[24] G. Parkin, *Chem. Rev*., 2004, **104**, 699-767.

[25] X. P. Zhang, R. van Eldik, T. Koike and E. Kimura, *Inorg. Chem*., 1993, **32**, 5749-5755.

[26] X. P. Zhang and R. van Eldik, *Inorg. Chem*. 1995, **34**, 5606-5614.

[27] (A) M. J. Frisch, G. W. Trucks, H. B. Schlegel, G. E. Scuseria, M. A. Robb, J. R. Cheeseman, J. A. Montgomery, Jr., T. Vreven, K. N. Kudin, J. C. Burant, J. M. Millam, S. S. Iyengar, J. Tomasi, V. Barone, B. Mennucci, M. Cossi, G. Scalmani, N. Rega, G. A. Petersson, H. Nakatsuji, M. Hada, M. Ehara, K. Toyota, R. Fukuda, J. Hasegawa, M. Ishida, T. Nakajima, Y. Honda, O. Kitao, H. Nakai, M. Klene, X. Li, J. E. Knox, H. P. Hratchian, J. B. Cross, V. Bakken, C. Adamo, J. Jaramillo, R. Gomperts, R. E. Stratmann, O. Yazyev, A. J. Austin, R. Cammi, C. Pomelli, J. W. Ochterski, P. Y. Ayala, K. Morokuma, G. A. Voth, P. Salvador, J. J. Dannenberg, V. G. Zakrzewski, S. Dapprich, A. D. Daniels, M. C. Strain, O. Farkas, D. K. Malick, A. D. Rabuck, K. Raghavachari, J. B. Foresman, J. V. Ortiz, Q. Cui, A. G. Baboul, S. Clifford, J. Cioslowski, B. B. Stefanov, G. Liu, A. Liashenko, P. Piskorz, I. Komaromi, R. L. Martin, D. J. Fox, T. Keith, M. A. Al-Laham, C. Y. Peng, A. Nanayakkara, M. Challacombe, P. M. W. Gill, B. Johnson, W. Chen, M. W. Wong, C. Gonzalez, and J. A. Pople, Gaussian 03, Revision C.02, Gaussian, Inc., Wallingford CT, 2004. (B) M. J. Frisch, G. W. Trucks, H. B. Schlegel, G. E. Scuseria, M. A. Robb, J. R. Cheeseman, G. Scalmani, V. Barone, B. Mennucci, G. A. Petersson, H. Nakatsuji, M. Caricato, X. Li, H. P. Hratchian, A. F. Izmaylov, J. Bloino, G. Zheng, J. L. Sonnenberg, M. Hada, M. Ehara, K. Toyota, R. Fukuda, J. Hasegawa, M. Ishida, T. Nakajima, Y. Honda, O. Kitao, H. Nakai, T. Vreven, J. A. Montgomery, Jr., J. E. Peralta, F. Ogliaro, M. Bearpark, J. J. Heyd, E. Brothers, K. N. Kudin, V. N. Staroverov, R. Kobayashi, J. Normand, K. Raghavachari, A. Rendell, J. C. Burant, S. S. Iyengar, J. Tomasi, M. Cossi, N. Rega, J. M. Millam, M. Klene, J. E. Knox, J. B. Cross, V. Bakken, C. Adamo, J. Jaramillo, R. Gomperts, R. E. Stratmann, O. Yazyev, A. J. Austin, R. Cammi, C. Pomelli, J. W. Ochterski, R. L. Martin, K. Morokuma, V. G. Zakrzewski, G. A. Voth, P. Salvador, J. J. Dannenberg, S. Dapprich, A. D. Daniels, Ö. Farkas, J. B. Foresman, J. V. Ortiz, J. Cioslowski, and D. J. Fox, Gaussian 09, Revision B.01 Gaussian, Inc., Wallingford CT, 2009.

[28] (a) A. D. Becke, *J. Chem. Phys*., 1993, **98**, 5648-5652; (b) C. Lee, W. Yang, and R. G. Parr, *Phys. Rev. B*, 1988, **37**, 785-789.

[29] P. E. Haffner and J. E. Coleman, *J. Biol. Chem*., 1973, **248**, 6630-6636.

[30] S. F. Boys and F. Bernardi, *Mol. Phys*., 1970, **19**, 553-566.

[31] N. E. Schultz, Y. Zhao, and D. G. Truhlar*, J. Phys. Chem. A*, 2005, **109**, 11127-11143.

[32] V. Barone and M. Cossi, *J. Phys. Chem. A*., 1988, **102**, 1995-2001.

[33] (a) V. Barone, M. Cossi, and J. Tomassi, *J. Comput. Chem*., 1998, **19**, 404-417; (b) T. Mineva, N. Russo, and E. Sicilia, *J. Comput. Chem*., 1998, **19**, 290-299.

[34] V. Barone, M. Cossi, and J. Tomasi, *J. Chem. Phys*., 1997, **107**, 3210-3221.

[35] A. K. Rappe, C. J. Casewit, K. S. Colwell, W. A. Goddard III, and W. M. Skiff, *J. Am. Chem. Soc*., 1992, **114**, 10024-10035.

[36] A. E. Reed, R. B. Weinstock, and F. Weinhold, *J. Chem. Phys*., 1985, **83**, 735-746.

[37] F. da Silva Miranda, A. M. Signori, J. Vicente, B. de Souza, J. P. Priebe, B. Szpoganicz, N. Sanchez Goncalves, and A. Neves, *Tetrahedron*, 2008, **64**, 5410-5415.

[38] V. O. Rodinov, S. I. Presolski, S. Gardinier, Y.-H. Lim, and M. G. Finn*, J. Am. Chem. Soc*., 2007, **129**, 12696-12704.

[39] (a) I. Bertini, G. Lanini and C. Luchinat, *J. Am. Chem. Soc*., 1983, **105**, 5116-5118; (b) V. Yachandra, L. Powers and T. G. Spiros, *J. Am.Chem. Soc*., 1983, **105**, 6596-6604.

[40] (a) M. Sola, A. Lledos, M. Duran and J. Bertran, *J. Am. Chem. Soc*., 1992, **114**, 869-877; (b) Y.-J. Zheng and K. M. Merz, *J. Am. Chem. Soc*., 1992, **114**, 10498-10507; (c) J. Aqvist, M. Fothergill and A. Warshel, *J. Am. Chem. Soc*., 1993, **115**, 631-635; (d) D. Lu and G. A. Voth, *J. Am. Chem. Soc*., 1998, **120**, 4006-4014; (e) M. J. Loferer, C. S. Tautermann, H. H. Loeffler and K. R. Liedl, *J. Am. Chem. Soc*., 2003, **125**, 8921-8927; (f) A. Bottoni, C. Z. Lanza, G. P. Miscione and D. Spinelli, *J. Am. Chem. Soc*., 2004, **126**, 1542-1550; (g) G. P. Miscione, M. Stenta, D. Spinelli, E. Anders and A. Bottoni, *Theor. Chem. Acc*., 2007, **118**, 193-201.

[41] (a) D. R. Garmer and M. Krauss, *J. Am. Chem. Soc*., 1992, **114**, 6487-6493; (b) T. Marino, N. Russo and M. Toscano, *J. Am. Chem. Soc*., 2005, **127**, 4242-4253.

[42] M. Brauer, J. L. Perez-Lustres, J. Weston, and E. Anders, *Inorg. Chem.*, 2002, **41**, 1454-1463.

[43] J. F. Domsic, B. S. Avvaru, C. U. Kim, S. M. Gruner, M. Agbandje-McKenna, D. N. Silverman, and R. McKenna, *J. Biol. Chem*., 2008, **283**, 30766-30771.

[44] K. M. Merz, R. Hoffmann, M. J. S. Dewar, *J. Am. Chem. Soc*., 1989, **111**, 5636-5649.

[45] C. S. Tautermann, M. J. Loferer, A. F. Voegele, and K. R. Liedl, *J. Phys. Chem. B*, 2003, **107**, 12013-12020.

[46] (a) R. Han, A. Looney, K. McNeill, G. Parkin, A. L. Rheingold, and B. S. Haggerty, *J. Inorg. Biochem*., 1993, **49**, 105-121. (b) N. Kitajima, S. Hikichi, M. Tanaka, and T. Moro-oka, *J. Am. Chem. Soc*., 1993, **115**, 5496-5508.

[47] C. Bergquist, T. Fillebeen, M. M. Morlok, and G. Parkin, *J. Am. Chem. Soc*., 2003, **125**, 6189-6199.

[48] B. Sjoeblom, M. Polentarutti, and K. Djinovic-Carugo, *Proc. Natl. Acad. Sci. USA*., 2009, **106**, 10609-10613.

[49] P. A. Mazumdar, D. Kumaran, A. K. Das, S. Swaminathan, *Acta. Crystallogr. Sect. F*, 2008, **64**, 163-166.

[50] K. Hakansson, C. Briand, V. Zaitsev, Y. Xue, A. Liljas, *Acta, Crystallogr. Sect. D.,* 1994, **50**, 101-104.

[51] Y. Xue, A. Liljas, B.-H. Jonsson, and S. Lindskog, *Proteins, Struc., Funct., and Genetics*., 1993, **17**, 93-106.

[52] Z. Liang, Y. Xue, G. Behravan, B.-H. Jonsson, and Lindskog, *Eur. J. Biochem*., 1993, **211**, 821-827.

[53] K. Hakansson and A. Wehnert, *J. Mol. Biol*., 1992, **228**, 1212-1218.

[54] P. C. Kunz, A. Zribi, W. Frank, and W. Klaui, *Z. Anong. Allg. Chem*., 2007, **633**, 955-960.

[55] Y. Fan and Y. Q. Gao, *J. Am. Chem. Soc.,* 2007, **129**, 905-913.

[56] X. Yin, C. Lin, Z. Zhou, W. Chen, S. Zhu, H. Lin, X. Su, and Y. Chen, *Transit. Metal. Chem.,* 1999, **24**, 537-540.

[57] K. Nakata, J. Shimomura, N. Shiina, M. Izumi, K. Ichikawa, and M. Shiro, *J. Inorg. Biochem*., 2002, **89**, 255-266.

[58] M. Mauksch, M. Brauer, J. Weston, and E. Anders, *ChemBioChem*, 2001, **2**, 190-198.

[59] E. Kimura, T. Koike, and K. Toriumi, *Inorg. Chem*., 1988, **27**, 3687-3688.

[60] L. Koziol, C. A. Valdez, S. E. Baker, E. Y. Lau, W. C. Floyd, III, S. E. Wong, J. H. Satcher, Jr., F. C. Lightstone, and R. D. Aines, *Inorg. Chem*., 2012, **51**, 6803-6812.

[61] R. S. Brown, N. J. Curtis, and J. Huguet, *J. Am. Chem. Soc.*, 1981, **103**, 6953-6959.

[62] K. Hakansson, A. Wehnert, and A. Liljas, *Acta Crystallogr. Sect. D*, 1994, **50**, 93-100.

[63] I. Simonsson, B.-H. Jonsson, and Lindskog, Eur*. J. Biochem.*, 1979, **93**, 409-417.

[64] J. F. Krebs, J. A. Ippolito, D. W. Christianson, and C. A. Fierke, *J. Biol. Chem*., 1993, **268**, 27458-27466.

[65] K. M. Merz and L. Banci, *J. Am. Chem. Soc*., 1997, **119**, 863-871.

[66] G. Behravan, B.-H. Jonsson, and S. Lindskog, *Eur. J. Biochem*., 1990, **190**, 351-357.

[67] S. Z. Fisher, C. M. Maupin, M. Budayova-Spano, L. Govindasamy, C. K. Tu, M. Agbandje-McKenna, D. N. Silverman, G. A. Voth, and R. McKenna, *Biochemistry*, 2007, **46**, 2930-2937.

[68] M. J. Loeferer, C. S. Tautemann, H. H. Loeffler, and K. R. Liedl, *J. Am. Chem. Soc*., 2003, **125**, 8921-8927.

[69] (a) I. Bertini, G. Canti, C. Luchinat, and F. Mani, *Inorg. Chem*., 1981, **20**, 1670-1673. (b) C. Benelli, I. Bertini, M. Di Vaira, and F. Mani, *Inorg. Chem*., 1984, **23**, 1422-1425.

[70] R. Davy, *Energy Procedia*, 2009, **1**, 885-892.

[71] S. R. MacAuldey, S. A. Zimmerman, E. E. Apolinario, C. Evilia, Y.-M. Hou, J. G. Perry, and K. R. Sower, *Biochemistry*, 2009, **48**, 817-819.

[72] B. E. Alber, C. M. Colangelo, J. Dong, C. M. V. Stalhandske, T. T. Baird, C. Tu, C. A. Fierke, D. N. Silverman, R. A. Scott, and J. G. Ferry, *Biochemistry*, 1999, **38**, 13119-13128.

[73] T. M. Iverson, B. E. Alber, C. Kisker, J. G. Ferry, and D. C. Rees, *Biochemistry*, 2000, **39**, 9222-9231.

[74] A. Innocenti, S. Zimmerman, J. G. Ferry, A. Scozzafava, and C. T. Supuran, *Bioorg. and Med. Chem. Lett.*, 2004, **14**, 3327-3331.

FIGURE CAPTIONS

Figure 1. Schematic drawing of the structures of 1,5,9-triazacyclododedacane (**A**) and 1,4,7,10-tetraazacyclododedacane (**B**) which are denoted **N3** and **N4** in the text, respectively. Panel (**C**) shows how the atoms are denoted in the text. The structures of tris(4,5-dimethyl-2-imidazolyl)phosphine (**D**) and tris(2-benzimidazlylmethyl)amine (**E**) are denoted **Phen** and **Ben** in the text, respectively.

Figure 2. Calculated structures for the zinc complexes of **N3**, **N4, Phen,** and **Ben** complexes during the nucleophilic attack portion of the hydration reaction of CO_2 when forming the encounter complex (EC), first transition state (TS1), Lindskog intermediate (I1), and Lipscomb intermediate (I2). Distances are listed in angstroms and values in the parenthesis are the corresponding distances for the cobalt complexes.

Figure 3. Relative energy of the calculated stationary points for **N3** in Panel (**A**), **N4** in Panel (**B**), **Phen** in Panel (**C**), and **Ben** in Panel (**D**) along the reaction coordinate relative to the separated reactants (SR). The energies for the zinc complexes are represented by the gray line and the cobalt complexes by the black line.

Figure 4. Calculated structures for the transition state (TS2) separating the Lindskog (I1) and Lipscomb (I2) intermediates for **N4**-Zn (**A**) and **N4**-Co (**B**). The angle listed is formed by the point generated by the center of mass of the ring nitrogens-metal ion-coordinating oxygen of bicarbonate.

Figure 5. Optimized structures of I2 interacting with a single water molecule for **N3** (**A**), **N4** (**B**), **Phen** (**C**), and **Ben** (**D**), respectively. Numerical values are in angstroms.

Figure 6. Optimized structures of the **Phen**-bicarbonate-water structures. Panel (**A**) is the lowest energy structure and has the water in the axial position. The angle formed by the imidazole nitrogen (arrow)-Zn-oxygen (water) is almost linear. Panel (**B**) has the bicarbonate in the axial position. Panel (**C**) shows an overlay of the two structures and how interconversion between the two geometries can occur.

Figure 7. Comparison of calculated structures for **Phen**-Zn with bicarbonate and X-ray crystal structures of carbonic anhydrase II interacting with acetate. Panels (**A**) and (**B**) show wild-type carbonic anhydrase II and Panel (**C**) show the E106Q mutant.

Figure 8. Panel (**A**) shows the low energy structure of **Phen**-Co interacting with water (I3). Panel (**B**) shows an overlay of the **Phen**-Co (I3, green) structure with the wild-type (zinc) carbonic anhydrase with acetate (1XEG, cyan). Panel (**C**) shows an octahedral geometry for bicarbonate and water bound to cobalt. Panel (**D**) shows the arrangement of ligands (water and bicarbonate) around the metal ion in the X-ray crystal structure of cobalt carbonic anhydrase (1CAH).

Figure 9. Calculated transition state structures (TS3) for displacement of bicarbonate by a water molecule for **N3**-Zn (**A**), **N4**-Zn (**B**), and **Phen**-Zn (**D**). Numerical values are in angstroms and values in parenthesis are the corresponding values for the cobalt structures.

Figure 10. Optimized geometries for the bicarbonate and water bound to Ben-Zn with the water in the axial position (**A**) and equatorial position (**B**). Panel (**C**) and (**D**) show the corresponding transition states for (**A**) and (**B**), respectively. Values are in angstroms and values in parenthesis are for the corresponding cobalt structures.

Figure 11. Relative energies to the separated reactants from single point solvation (CPCM) calculations using the gas-phase stationary points for **N3**-Zn (black) and **N3**-Co (gray) are shown in Panel (**A**) and **N4**-Zn (black) and **N4**-Co (gray) are shown in Panel (**B**).

Figure 12. X-ray crystal structures of the active site of Zn-Cam (1QRL) and Co-Cam (1QRE) binding bicarbonate, are shown in **(A)** and **(B)**, respectively. Numerical values are the oxygen to metal distances and are in angstroms.

Figure 1

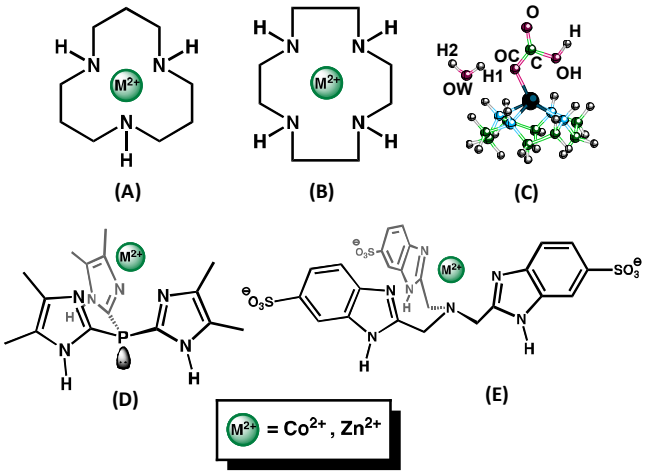

Figure 2

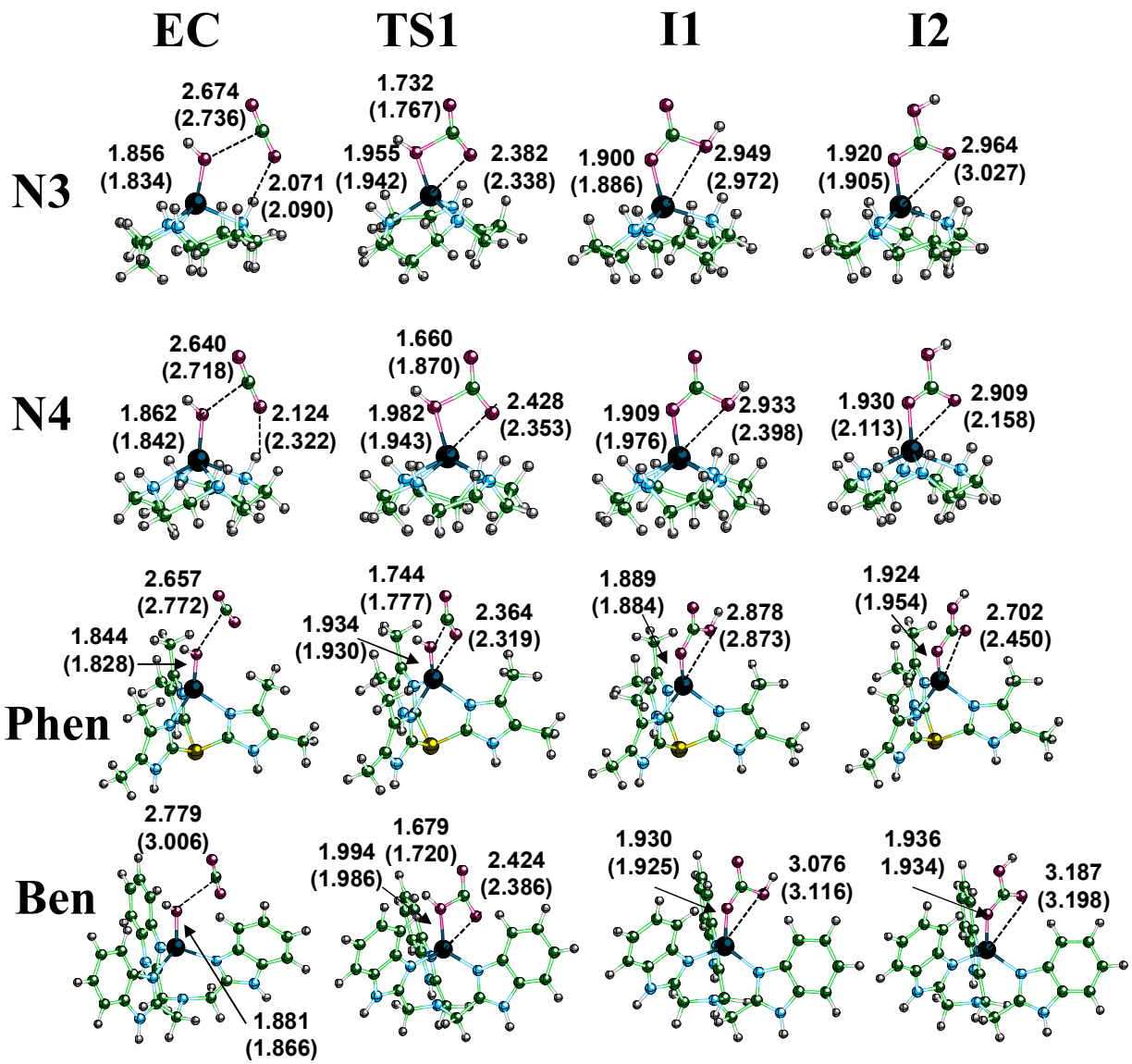
EC
TS1
I1
I2
N3
2.674
(2.736)
1.856
(1.834)
2.071
(2.090)
1.732
(1.767)
1.955
(1.942)
2.382
(2.338)
1.900
(1.886)
2.949
(2.972)
1.920
(1.905)
2.964
(3.027)
N4
2.640
(2.718)
1.862
(1.842)
2.124
(2.322)
1.660
(1.870)
1.982
(1.943)
2.428
(2.353)
1.909
(1.976)
2.933
(2.398)
1.930
(2.113)
2.909
(2.158)
Phen
2.657
(2.772)
1.844
(1.828)
1.744
(1.777)
1.934
(1.930)
2.364
(2.319)
1.889
(1.884)
2.878
(2.873)
1.924
(1.954)
2.702
(2.450)
Ben
2.779
(3.006)
1.881
(1.866)
1.679
(1.720)
1.994
(1.986)
2.424
(2.386)
1.930
(1.925)
3.076
(3.116)
1.936
1.934
3.187
(3.198)

Figure 3

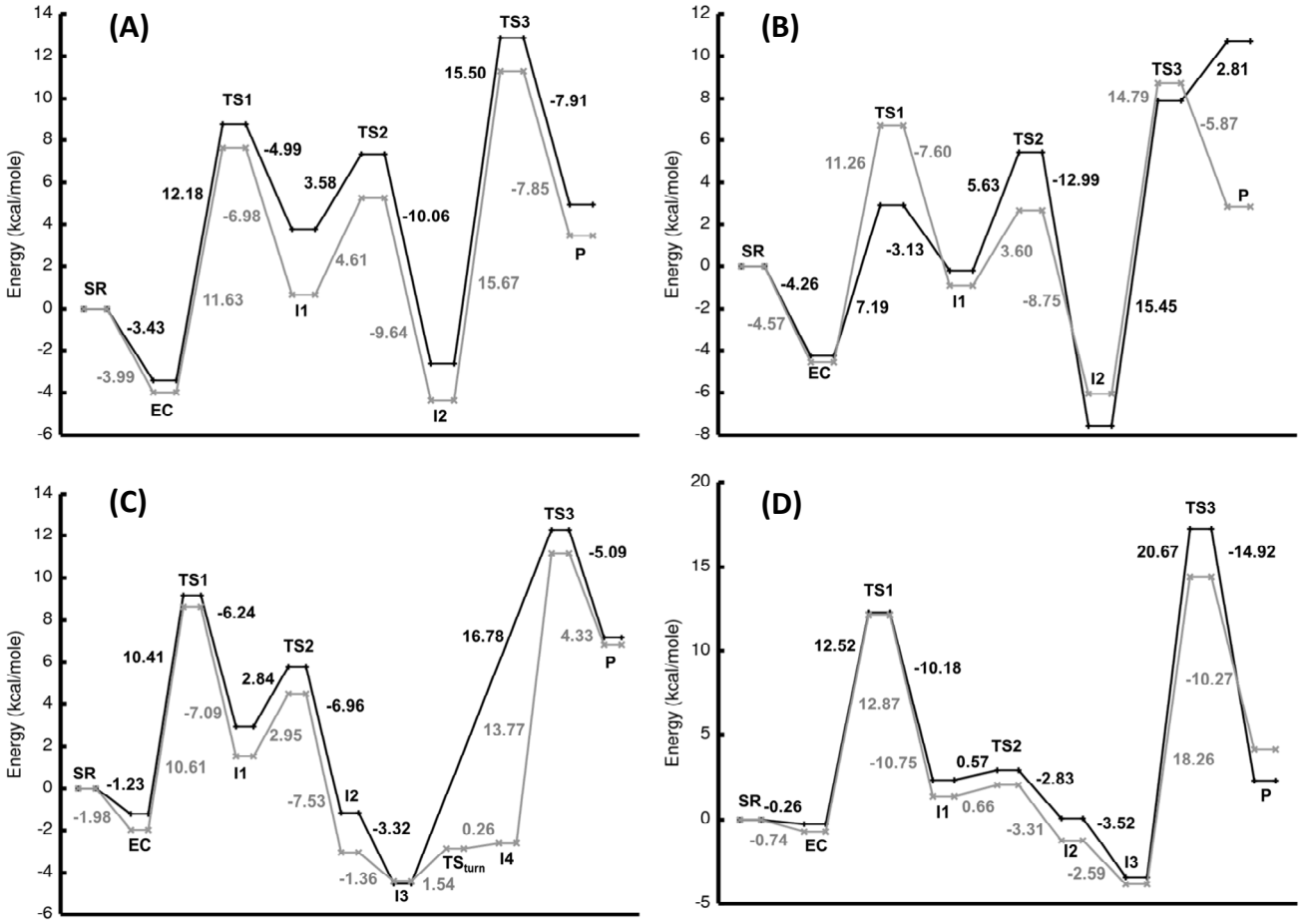
(A)
Energy (kcal/mole)
SR
-3.43
-3.99
EC
12.18
11.63
TS1
-4.99
-6.98
I1
3.58
4.61
TS2
-10.06
-9.64
I2
15.50
15.67
TS3
-7.91
-7.85
P
(B)
Energy (kcal/mole)
SR
-4.26
-4.57
EC
7.19
11.26
TS1
-3.13
-7.60
I1
5.63
3.60
TS2
-12.99
-8.75
I2
14.79
15.45
TS3
2.81
-5.87
P
(C)
Energy (kcal/mole)
SR
-1.23
-1.98
EC
10.41
10.61
TS1
-6.24
-7.09
I1
2.84
2.95
TS2
-6.96
-7.53
I2
-3.32
-1.36
I3
16.78
1.54
TS$_{turn}$
0.26
13.77
I4
4.33
TS3
-5.09
P
(D)
Energy (kcal/mole)
SR
-0.26
-0.74
EC
12.52
12.87
TS1
-10.18
-10.75
I1
0.57
0.66
TS2
-2.83
-3.31
I2
-3.52
-2.59
I3
20.67
18.26
TS3
-14.92
-10.27
P

Figure 4

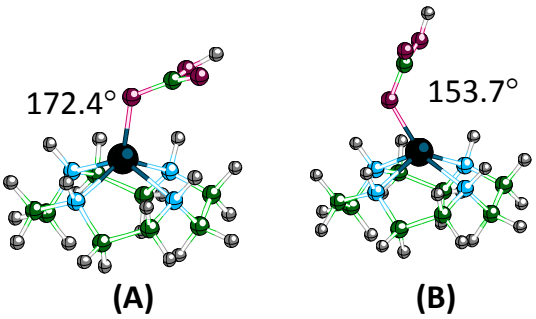

Figure 5

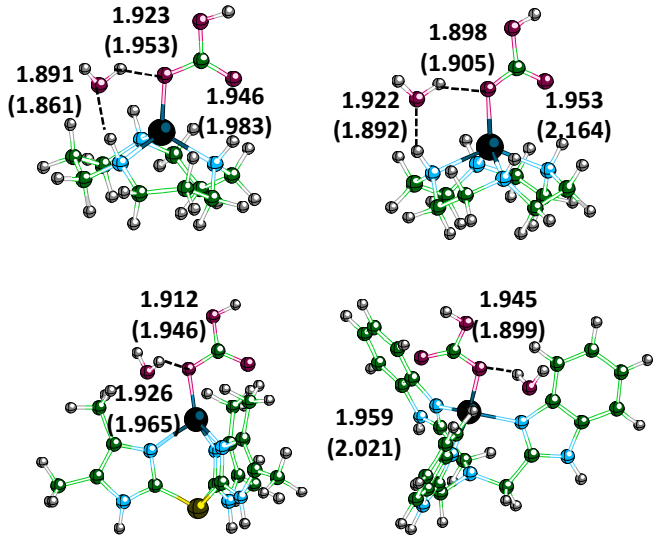
1.923
(1.953)
1.891
(1.861)
1.946
(1.983)
1.898
(1.905)
1.922
(1.892)
1.953
(2.164)
1.912
(1.946)
1.926
(1.965)
1.945
(1.899)
1.959
(2.021)

Figure 6

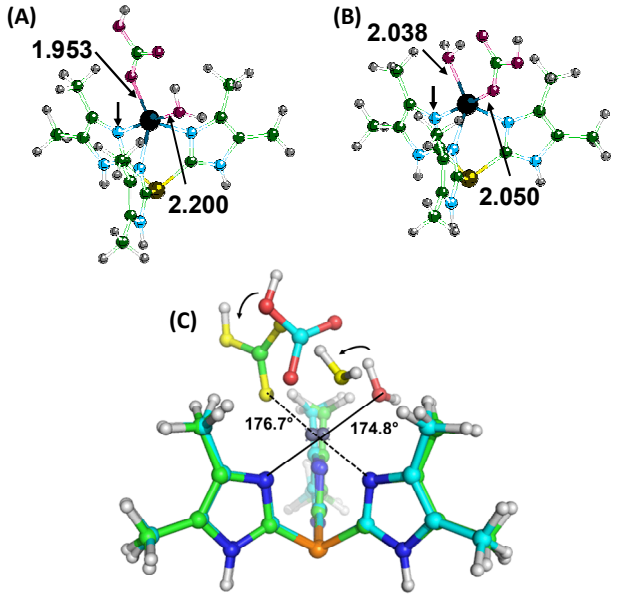

Figure 7

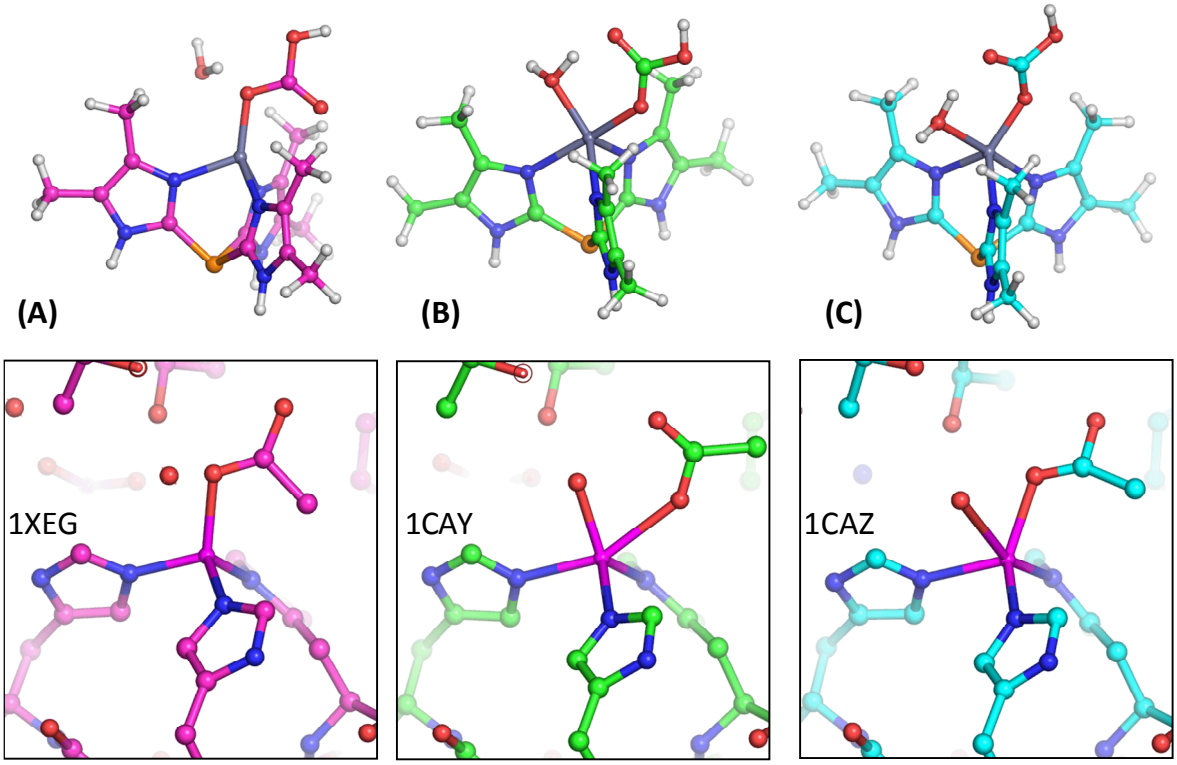

Figure 8

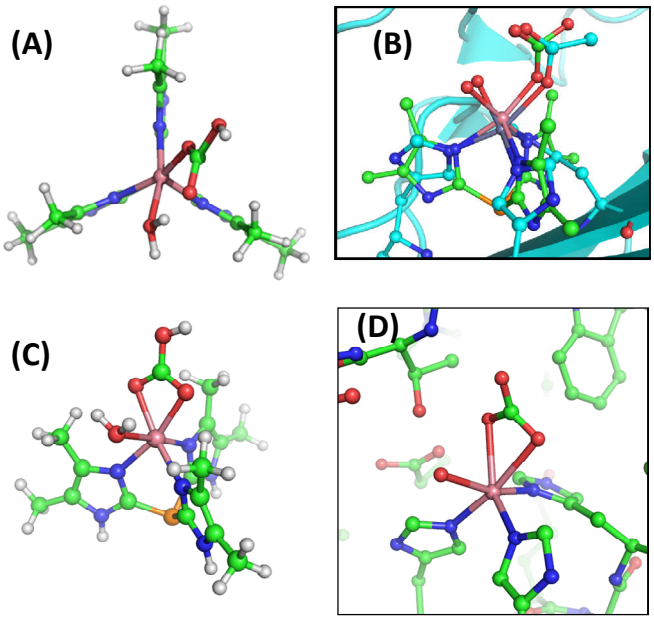

Figure 9

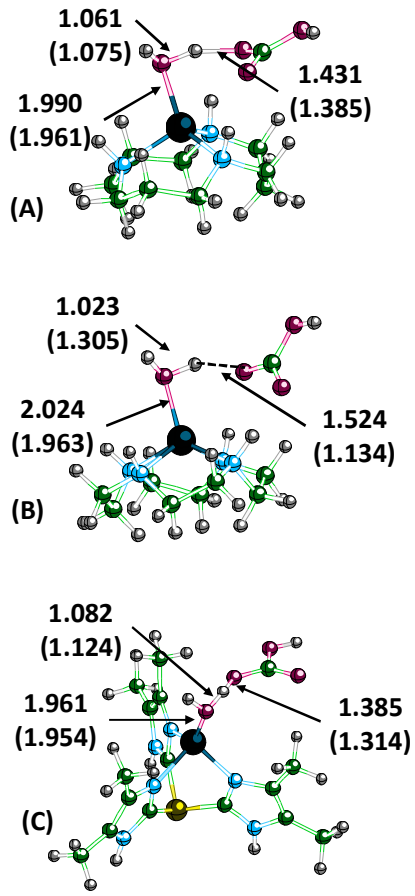
1.061
(1.075)
1.431
(1.385)
1.990
(1.961)
(A)
1.023
(1.305)
2.024
(1.963)
1.524
(1.134)
(B)
1.082
(1.124)
1.961
(1.954)
1.385
(1.314)
(C)

Figure 10

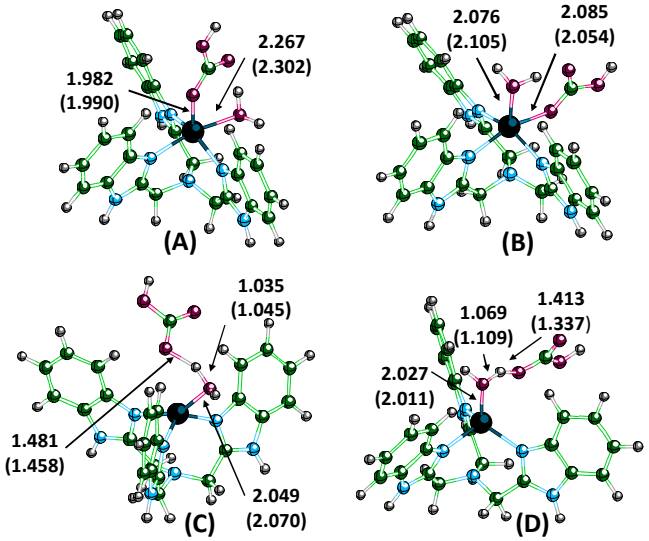
1.982
(1.990)
2.267
(2.302)
(A)
2.076
(2.105)
2.085
(2.054)
(B)
1.035
(1.045)
1.481
(1.458)
2.049
(2.070)
(C)
1.069
(1.109)
1.413
(1.337)
2.027
(2.011)
(D)

Figure 11

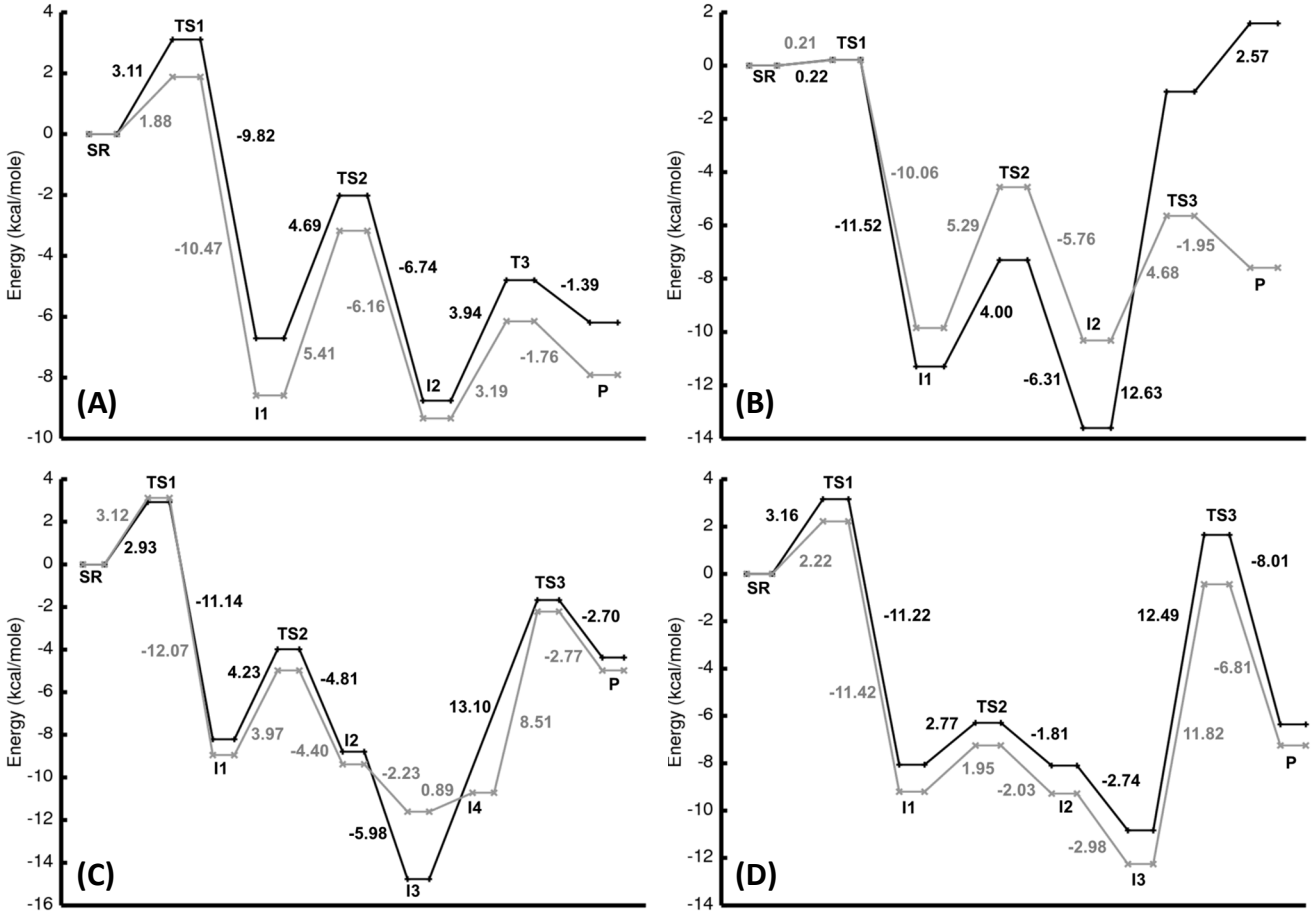
Energy (kcal/mole)
(A)
SR
TS1
I1
TS2
I2
T3
P
3.11
1.88
-9.82
-10.47
4.69
5.41
-6.74
-6.16
3.94
3.19
-1.39
-1.76
(B)
SR
TS1
I1
TS2
I2
TS3
P
0.21
0.22
-10.06
-11.52
5.29
4.00
-5.76
-6.31
2.57
12.63
-1.95
4.68
(C)
SR
TS1
I1
TS2
I2
I3
I4
TS3
P
3.12
2.93
-11.14
-12.07
4.23
3.97
-4.81
-4.40
-2.23
-5.98
0.89
13.10
8.51
-2.70
-2.77
(D)
SR
TS1
I1
TS2
I2
I3
TS3
P
3.16
2.22
-11.22
-11.42
2.77
1.95
-1.81
-2.03
-2.74
-2.98
12.49
11.82
-8.01
-6.81

Figure 12